ACS OMEGA

http://pubs.acs.org/journal/acsodf

Article

Insight into the Conformational Transitions of Serine Acetyl Transferase Isoforms in *E. histolytica*: Implications for Structural and Functional Balance

Danish Idrees, Ahmad Abu Turab Naqvi, Md Imtaiyaz Hassan, Faizan Ahmad, and Samudrala Gourinath*

Cite This: *ACS Omega* 2022, 7, 24626−24637

Read Online

ACCESS | Metrics & More | Article Recommendations | Supporting Information

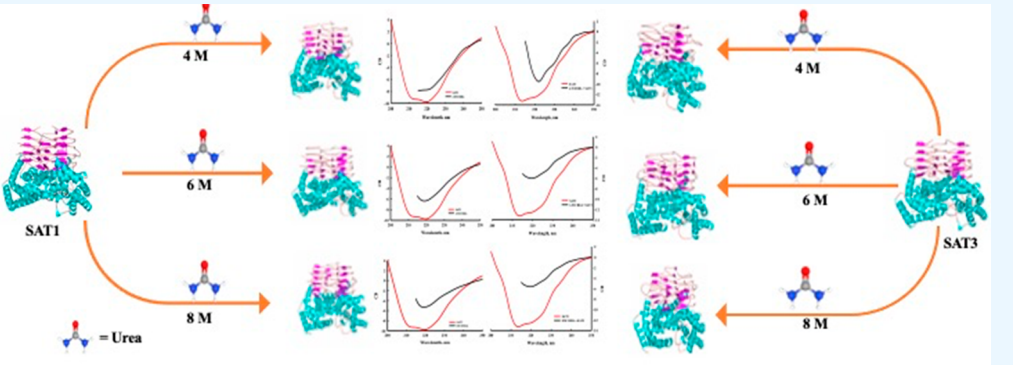

ABSTRACT: Serine acetyl transferase (SAT) is one of the crucial enzymes in the cysteine biosynthetic pathway and an essential enzyme for the survival of *Entamoeba histolytica*, the causative agent of amoebiasis. *E. histolytica* expresses three isoforms of SAT, where SAT1 and SAT2 are inhibited by the final product cysteine, while SAT3 is not inhibited. SAT3 has a slightly elongated C-terminus compared to SAT1. To understand the stability and conformational transition between two secondary structures of proteins, we measured the effect of urea, a chemical denaturant, on two isoforms of SAT (SAT1 and SAT3) of *E. histolytica*. The effect of urea on the structure and stability of SAT1 and SAT3 was determined by measuring changes in their far-UV circular dichroism (CD), Trp fluorescence, and near-UV absorption spectra. The urea-induced normal transition curves suggested that the structural transition is reversible and follows a two-state process. Analysis of the urea-induced transition of all optical properties for the stability parameters ΔG_D° (Gibbs free energy change (ΔG_D) in the absence of urea), m (dependence of ΔG_D on urea concentration), and C_m (midpoint of urea transition) suggested that SAT1 is more stable than SAT3. Characterization of the end product of the urea-induced transition of both proteins by the far-UV CD and Trp-fluorescence and near-UV absorbance suggested that urea causes α-helix to β-sheet transition and burial of Trp residues, respectively. To support the *in vitro* findings, 100 ns molecular dynamics simulations (*in silico* study) were performed. Both the spectroscopic and molecular dynamics approaches clearly indicated that SAT1 is more stable than SAT3. SAT3 has evolved to escape the feedback inhibition to keep producing cysteine, but in the process, it compromises its structural stability relative to SAT1.

1. INTRODUCTION

Entamoeba histolytica is an enteric protist parasite that causes amebic colitis and extra intestinal abscesses (i.e., hepatic, pulmonary, and cerebral).[1,2] The cysteine biosynthetic pathway is important for the growth, survival, and pathogenicity of *E. histolytica* as it is involved in the synthesis of cysteine which serves crucial roles as antioxidative agents and as a sulfur source for various biomolecules like thiols (glutathione, trypanothione, mycothiol), biotin, Fe−S clusters, and thiamine.[1,3] Serine acetyltransferase (SAT1 EC 2.3.1.30) is an enzyme of the L-cysteine biosynthesis pathway, which catalyzes the acetyl-CoA dependent acetylation of the side chain hydroxyl group of L-serine to form O-acetylserine. Another enzyme of the pathway is O-acetyl serine sulfhydrylase (OASS) that further catalazes the insertion of sulfide into OAS and generate cysteine with the release of acetate.[4] The cysteine biosynthetic pathway is regulated by several mechanisms, including feedback inhibition of SAT by cysteine.[1,5] *E.*

Received: April 20, 2022
Accepted: June 23, 2022
Published: July 7, 2022

histolytica has three isoforms of SAT (SAT1, SAT2, and SAT3). SAT1 shows 78% sequence homology with SAT2 and 48% with SAT3. These three isoforms are differing in length and show differences in sensitivity to the feedback inhibitor L-cysteine.[4] SAT1 and SAT2 are inhibited by Cys via a feedback mechanism, although SAT3 is insensitive to this inhibition.[6]

Biological studies indicate that SAT3 is very crucial for survival, while SAT1 and SAT2 deleted mutant strains can still survive.[7] SAT1 is a trimeric protein, and its protomer structure contains two domains, an N-terminal α-helix-rich domain composed of a collective of eight α-helices responsible for oligomerization and a C-terminal left handed β-helical domain comprised predominantly of 14 β strands.[8] Like SAT1, SAT3 is also trimeric, and its N-terminal domain is highly variable in structure and charge distribution, which plays a role in not forming hexameric structures as seen in *E. coli* and other structures. The C-terminal domain is highly conserved in all organisms and plays a role in trimerization,[8] while the C-terminal end is highly diverse. Especially *E. histolytica* SAT3 has a long C-terminal end which is swapping over other monomers.[8]

Most of the folding studies have been carried out on the monomeric proteins as a model to understand the folding pathway of proteins *in vitro*.[9,10] However, complicated oligomeric F proteins are also used to study the folding pathway.[11,12] The major secondary structural elements are β-sheets and α-helices that facilitate the organization of the three-dimensional (3D) conformation of proteins and peptides.[13] The proper folding of the protein is to adopt the native structure to perform normal functions, whereas misfolding is linked to malfunctions and aggregation as well as various neurodegenerative diseases in humans.[14,15] The conformational changes in human protein structure from α-helix to β-sheets are responsible for various neurodegenerative diseases.[16−18] However, understanding of the structural behavior of β-sheet assemblies in neurodegenerative diseases remains poorly understood.

Despite being vital for the survival of *E. histoyltica*, very little information is available on the stability and biophysical properties of SAT isoforms. In this study, we report biophysical and thermodynamic properties of SAT1 and SAT3 isoforms of *E. histolytica* measured by different spectroscopic techniques that were used to monitor the urea-induced transition of these isoforms. The structural characterization of the end product of this chemical denaturant-induced transition suggested that each isoform undergoes an α-helical → β-structure transition resembling neurodegenerative structural transition. 100 ns MD simulations at 300 K were also carried out in water and different concentrations of urea to establish a correlation between *in vitro* and *in silico* results. Both the spectroscopic and molecular dynamics studies clearly indicated that SAT1 is more stable than SAT3.

2. MATERIALS AND METHODS

2.1. Materials. Ultrapure-grade urea was purchased from MP Biomedicals (India) Pvt. Ltd. Oligonucleotide primers were supplied by Polaris Biosciences India Pvt. Ltd. Agarose, bacto-tryptone, and yeast extract were purchased from HiMedia Laboratories, India. *E. coli* strain DH5α was used for DNA amplification, and the *Escherichia coli* BL21 (DE3) strain was used for expression of the proteins. pET-21c, and pET-28b (Novagen, Wisconsin, USA) were used as expression vectors. DNA restriction enzymes (*Nhe1* and *Xho1*) and T4 DNA-ligase were purchased from Thermo Scientific, USA. Phusion and Dnazyme DNA polymerase (*Taq* polymerase) were obtained from Promega. Lysozyme was obtained from Amersham Pharmacia Biotech. All chemicals and reagents were of analytical grade and highly pure and were, therefore, used without further purifications.

2.2. Expression and Purifications. *SAT1* and *SAT3* genes were subcloned in pET-21c and pET-28b expression vectors, respectively. These constructs were transformed into *Escherichia coli* BL21 (DE3) cells, and freshly transformed *Escherichia coli* BL21 (DE3) cells were grown in LB media supplemented with 100 μg/mL ampicillin at 37 °C to an A_{600} (absorbance at 600 nm) of 0.6. Then cultures of both SAT1 and SAT3 were induced by 0.5 mM isopropyl β-D-1-thiogalactopyranoside (IPTG) for overexpression of proteins, and cultures were allowed to grow for another 3 h at 37 °C. Cells were harvested by centrifugation at 7000*g* for 7 min at 4 °C. The harvested cells were suspended in lysis buffer (50 mM Tris-HCl, pH 8.0, 500 mM NaCl, 5% (v/v) glycerol, 5 mM β-mercaptoethanol, 0.1 mg/mL lysozyme, 1 mM phenylmethanesulfonyl fluoride containing 1% (v/v) Triton X-100 and lysed with three cycles of flash-freezing in liquid nitrogen and thawing. The cell lysate was sonicated on ice and centrifuged at 12 000*g* for 30 min at 4 °C. The supernatant was collected and subjected to Ni-NTA affinity chromatography. Further, proteins were purified by gel filtration chromatography.[4,8]

2.3. Preparation of Stocks Solutions of Urea and Sample Preparation. The stock solution of 10 M urea was prepared in 50 mM Tris buffer at pH 8.0. The urea stock solution was always freshly prepared to avoid the production of cyanate ions, and its concentration was confirmed by refractive index.[19] For chemical-induced transition studies of SAT1 and SAT3, protein solutions with different concentrations of urea were prepared in a volumetric flask and incubated overnight, enough time for the completion of the transition.[20] A concentration of 8.6 μM of SAT1 and 7.90 μM of SAT3 proteins was used in all measurements. Urea was added in subsequent samples with a gradual increase in concentration from 0.25 to 8.0 M. The urea-induced transition was studied at pH 8.0 and 25 °C.

2.4. Circular Dichroism (CD) Measurements. Secondary structures of SAT1 and SAT3 were measured with a Jasco CD spectrometer (model J-1500) equipped with a Peltier type temperature controller. The far-UV CD spectra (250−200 nm) were recorded at 25 ± 0.1 °C using a cuvette of 1 mm path length. The protein concentration of both proteins used in these measurements was 8.6 μM of SAT1 and 7.90 μM of SAT3 in a buffer of 50 mM Tris at pH 8.0 and 150 mM NaCl. To monitor the effect of urea on the secondary structure of SAT1 and SAT3, far-UV CD spectra of each protein were recorded in the presence of different concentrations of the denaturant.[21] The recorded CD spectra were uploaded onto the K2D2 server to estimate the secondary structural content of the protein.[22] This server is based on the comparison of real and predicted values, by means of the Pearson correlation coefficient (r) and the root-mean-square deviation (RMSD) of proteins with known 3D structure. The raw CD data were converted to the mean residue ellipticity, $[\theta]$ (degree cm^2 dmol^{-1}), using the relation:

$$[\theta]_\lambda = \frac{M_o \theta_\lambda}{10lc} \quad (1)$$

https://doi.org/10.1021/acsomega.2c02467
ACS Omega 2022, 7, 24626−24637

where θ_λ is the observed ellipticity in millidegrees at wavelength λ nm, M_0 is the mean residue weight of the protein, c is the concentration of the protein in mg/mL, and l is the path length of the cell in cm.

2.5. Fluorescence Measurements. Fluorescence spectral measurements were carried out in a Jasco spectrofluorimeter (Model FP-6200) using a 3 mm quartz cell at 25 ± 0.1 °C. These measurements provide information on the tertiary structures of SAT1 and SAT3. Both excitation and emission slits were set at 5 nm bandwidth. The temperature of the sample cell was maintained by circulating water using an external thermostated water bath. In these experiments, protein samples were excited at 292 nm, and emission spectra were recorded in the range of 300−400 nm. The protein concentration used was 8.6 μM of SAT1 and 7.90 μM of SAT3, respectively. To see the effect of urea on the tertiary structure of SAT1 and SAT3, intrinsic (Trp) fluorescence spectra were recorded as a function of the denaturant concentration.

2.6. Absorption Measurements. Near-UV absorption spectra of SAT1 and SAT3 were measured in a Jasco UV/visible spectrophotometer (Jasco V-660, Model B028661152) equipped with Peltier temperature controller (ETCS-761). To monitor the effect of urea on the tertiary structures of SAT1 and SAT3, all spectra were recorded in the wavelength range 340−240 nm. For each measurement, 8.6 μM of SAT1 and 7.90 μM of SAT3 concentration of proteins were used. Difference spectra were obtained by subtracting the spectrum of the native protein from the spectrum of the protein in the presence of denaturants. Absorbance at a given wavelength λ nm was converted into the molar absorption coefficient (ε_λ). A transition curve was generated by plotting $\Delta\varepsilon_{287}$ as a function of [urea], the molar concentration of urea. For each sample, at least three independent measurements were performed and averaged for analysis.

2.7. Data Analysis. The isothermal transition curves of SAT1 and SAT3 induced by urea were analyzed assuming that the transition process is reversible and proceeds through a two-state mechanism (i.e., N (native) state ↔ D (denatured) state). $[\theta]_{222}$ was used to monitor the change in secondary structure, whereas $\Delta\varepsilon_{287}$ and F_{345} (fluorescence intensity at 345 nm) indicate the changes in the tertiary structure of the protein as an influence of urea.[19] All three optical properties ($[\theta]_{222}$, $\Delta\varepsilon_{287}$, and F_{345}) were plotted against [urea] to obtain the transition curves. Each transition curve was analyzed for the estimation of stability parameters[23] using a nonlinear least-squares method according to eq 2.[24] Transition curves of all three optical methods were fitted according to eq 2 and give the values of C and m.

$$y(\mathrm{d}) = \frac{y_N(\mathrm{d}) + y_D(\mathrm{d}) \times e^{[-(\Delta G_D^0 + m_d[\mathrm{d}])/RT]}}{1 + e^{[-(\Delta G_D^0 + m_d[\mathrm{d}])/RT]}} \quad (2)$$

where $y(\mathrm{d})$ is the optical property observed at [d], the molar concentration of the denaturant; $y_N(\mathrm{d})$ and $y_D(\mathrm{d})$ are optical properties of the native and denatured protein molecules at [d], respectively; $\Delta G_D{}^0$ is the value of the Gibbs free energy change (ΔG_D) in the absence of the denaturant; m_d is the slope ($\partial\Delta G_D/\partial[\mathrm{d}]$); R is the universal gas constant; and T denotes the temperature in Kelvin. It should be noted that the analysis transition curve was done assuming that unfolding is a two-state process and reversible and dependencies of $y_N(\mathrm{d})$ and $y_D(\mathrm{d})$ are linear (i.e., $y_N(\mathrm{d}) = a_N + b_N[\mathrm{d}]$ and $y_D(\mathrm{d}) = a_D + b_D[\mathrm{d}]$, where a and b are [d]-independent parameters, and subscripts N and D represent that these parameters are for the native and denatured protein molecules, respectively. At a given denaturant concentration, the fraction of the protein converted to β-structure f_β was estimated using the relation:

$$f_\beta = \frac{(y - y_N)}{(y_D - y_N)} = y - \frac{y - a_N + b_N[\mathrm{d}]}{(a_D - a_N) - (b_D + b_N)[\mathrm{d}]} \quad (3)$$

2.8. Molecular Dynamics Simulations. Molecular dynamics (MD) simulations of both SAT1 and SAT3 (three-dimensional structure was retrieved using the PDB ID 3PIB and PDB ID 7BW9, respectively) were performed using the GROMACS 2018.4 package. Both proteins were simulated in the presence of 4.0, 6.0, and 8.0 M urea. Before MD simulations, the structures were converted to GROMACS supported formats using the PDB 2gmx tool of GROMACS. The topology files were generated using the same tool with the force field GROMOS96 43a1. The structures then solvated using the aforementioned concentrations of urea, and water molecules were added. Subsequently, Na^+ and Cl^- ions were added in the system. Both the systems were then energy minimized using the steepest descent algorithm implemented in GROMACS for 100 ps (ps). Both the structures were analyzed for proper energy minimization. The energy minimized systems were then taken to equilibration using NVT and NPT methods for 100 ps each. The equilibrated systems were then considered for production MD of 100 ns (ns). Eventually, SAT1 in aqueous solution and in the presence of 4.0, 6.0, and 8.0 M urea were simulated for 100 ns. Similarly, SAT3 under the same solvent conditions was simulated for 100 ns. The trajectories generated after the 100 ns MD simulation of each system were then analyzed for structural changes and stability.

3. RESULTS AND DISCUSSION

Protein structure is crucial to its biological function. The various molecular interactions maintain the protein's proper folding and stability under physiological conditions. It is observed that cells and tissues under stress conditions due to a change in the solute concentration, high temperature, and some of the metabolic substances affect the activity and stability of proteins. The common chemical denaturants such as urea and GdmCl are used to induce the unfolding of protein to estimate the protein stability parameters. The protein folding and stability of monomeric protein studies have been carried out extensively. But, in recent years, the folding and stability of oligomeric proteins have been carried out to understand the structure−function relationship. *In vitro* and MD simulation approaches have been used to understand the mechanism of transition of proteins by urea.[20,25] In the present study, effects of urea on the stability of SAT1 and SAT3 were monitored using three optical methods and an MD simulation approach, which correlated very well. These results clearly indicate that SAT1 is more stable than SAT3, while functionally SAT3 is important for the survival of the organism.

3.1. Expression and Purifications of SAT1 and SAT3. SAT1 and SAT3 were expressed in *Escherichia coli* BL21 (DE3) cells, and these cells were harvested and resuspended in a lysis buffer. The cell lysate was sonicated on ice and centrifuged at 12 000*g* for 30 min at 4 °C. The supernatant was collected and subjected to Ni-NTA affinity chromatography. A

https://doi.org/10.1021/acsomega.2c02467
ACS Omega 2022, 7, 24626−24637

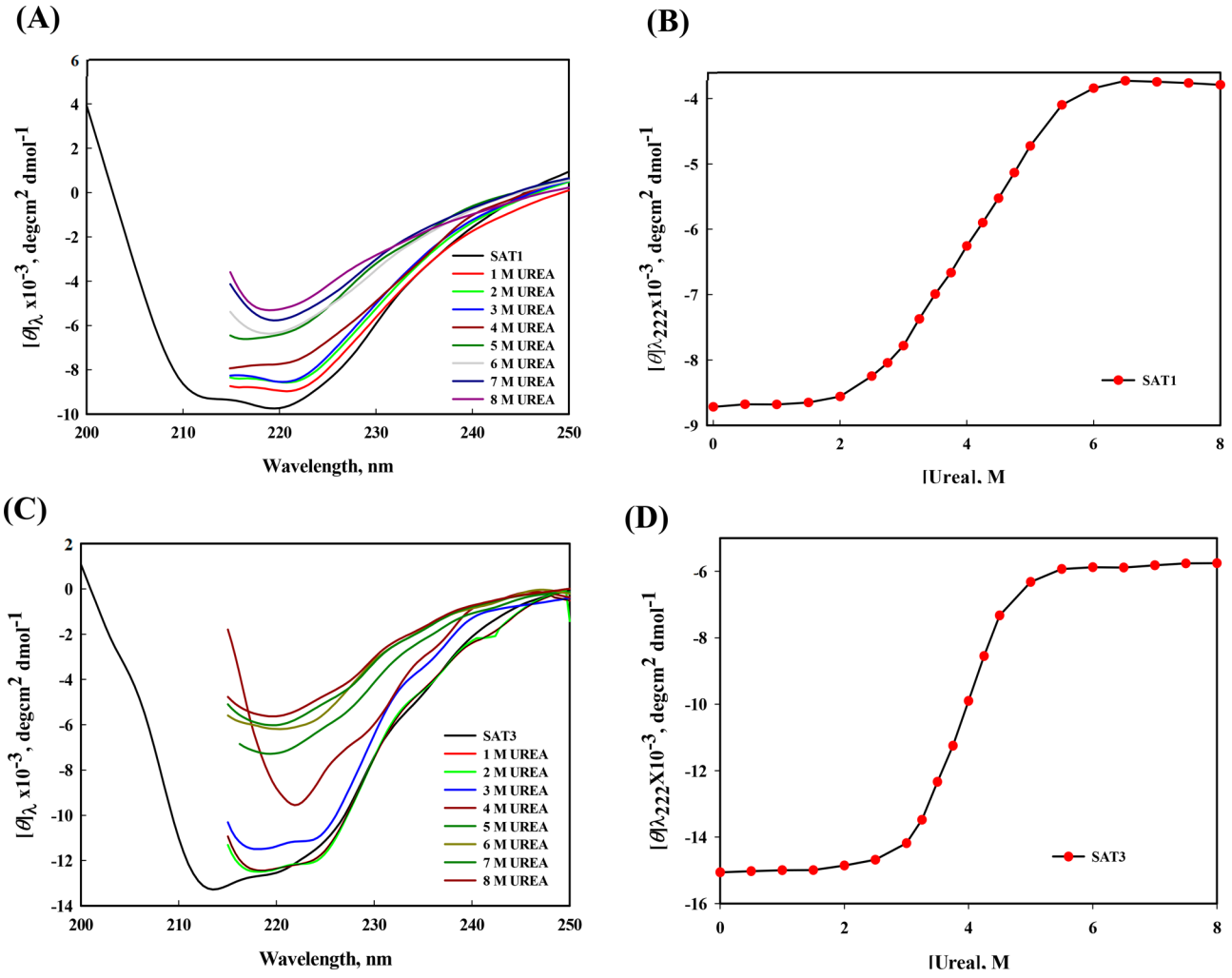

Figure 1. Far-UV CD spectra of SAT1 and SAT3 recorded as a function of increasing urea concentration at pH 8.0 and 25 °C. (A) Representative far-UV CD spectra of SAT1 in the presence of different concentrations of urea. (B) Urea-induced transition curve of SAT1 followed by observing changes in $[\theta]_{222}$. (C) Representative far-UV CD spectra of SAT3 in the presence of different concentrations of urea. (D) Urea-induced transition curve of SAT3 followed by observing changes in $[\theta]_{222}$.

clear supernatant of each SAT1 and SAT3 was passed through a Ni-NTA column, which was pre-equilibrated with the equlibration buffer (50 mM Tris-HCl, pH 8.0, 500 mM NaCl, 5% (v/v) glycerol, 5 mM β-mercaptoethanol, and 10 mM imidazole). This column was washed with five volumes of the wash buffer with 20 mM imidazole. The bound protein was eluted with 15 mL of elution buffer with 300 mM imidazole and collected in 1.5 mL fractions. The purity of eluted fractions of both proteins was checked on SDS-PAGE, and some impurities were found along with SAT1 and SAT3 proteins. Furthermore, proteins were subjected to gel filtration chromatography.[20,26] The proteins were concentrated using a centricon filter with a 30 kDa cutoff and loaded onto a HiLoad 16/60 Superdex 200 column (GE Healthcare) that had previously been equilibrated with a buffer of 50 mM Tris at pH 8.0, 150 mM NaCl, and 5% glycerol. Proteins were eluted at a flow rate of 1 mL/min. SAT1 was eluted at 72 mL, while SAT3 was at 84 mL. The elution profile shows that SAT1 and SAT3 exist as a trimer (Supplementary Figures S1 and S2). The purity of the proteins was checked on SDS-PAGE and concentrated using Centricon tubes (Amicon) to a final concentration of 12 mg/mL for SAT1 and 8 mg/mL for SAT3 as estimated by the Bradford method.

3.2. CD Measurements. The far-UV CD measurement is used to determine secondary structure.[27,28] It is also used to follow the transition between α-helix and β-structure. In the presence of different concentrations of urea, far-UV CD measurements were performed on SAT1 and SAT3 at 25 °C in the wavelength region 250−200 nm (Figure 1A and C). It should be noted that measurement of the CD spectrum of proteins is not possible beyond 215 nm due to a high photomultiplier voltage. Figure 1A and C show representative spectra, and other spectra are shown in Figure S2A and B (Supporting Information). The CD spectrum of each native protein was analyzed for the content of α-helix, β-structure, and unordered structure (random coil) using an online available program K2D2.[22] The analysis of the CD spectrum of the native SAT1 gave values of 20.2% for α-helix, 29.1% for β-sheet, and 50.7% random coil.[29] Analysis of the CD spectrum of the native SAT3 yielded values of 22.2% for α-helix, 27.1% for β-sheet, and 50.3% for random coil. Values of the secondary structural elements are in close agreement with those observed in the crystal structure.[26] These agreements mean that our CD measurements are accurate. We did not attempt to analyze CD spectra of proteins in the presence of the denaturant, for these spectra cannot be accurately obtained

https://doi.org/10.1021/acsomega.2c02467
ACS Omega 2022, 7, 24626−24637

Table 1. Thermodynamic Parameters Obtained from Urea-Induced Denaturation of SAT1 and SAT3 at pH 8.0 and 25 ± 0.1 °C

protein	SAT1			SAT3		
probes (urea)	ΔG_D°	m	C_m	ΔG_D°	m	C_m
$[\theta]_{222}$	5.91 ± 0.17	2.50 ± 0.11	2.35 ± 0.15	3.93 ± 0.13	1.09 ± 0.08	3.61 ± 0.16
F_{345}	4.85 ± 0.13	1.25 ± 0.09	3.88 ± 0.14	4.01 ± 0.15	1.02 ± 0.07	3.93 ± 0.20
$\Delta\varepsilon_{287}$	5.13 ± 0.15	1.37 ± 0.07	3.74 ± 0.17	3.88 ± 0.14	1.11 ± 0.04	3.40 ± 0.19
average	5.29 ± 0.15	1.70 ± 0.09	3.32 ± 0.15	3.94 ± 0.14	1.01 ± 0.06	3.65 ± 0.18

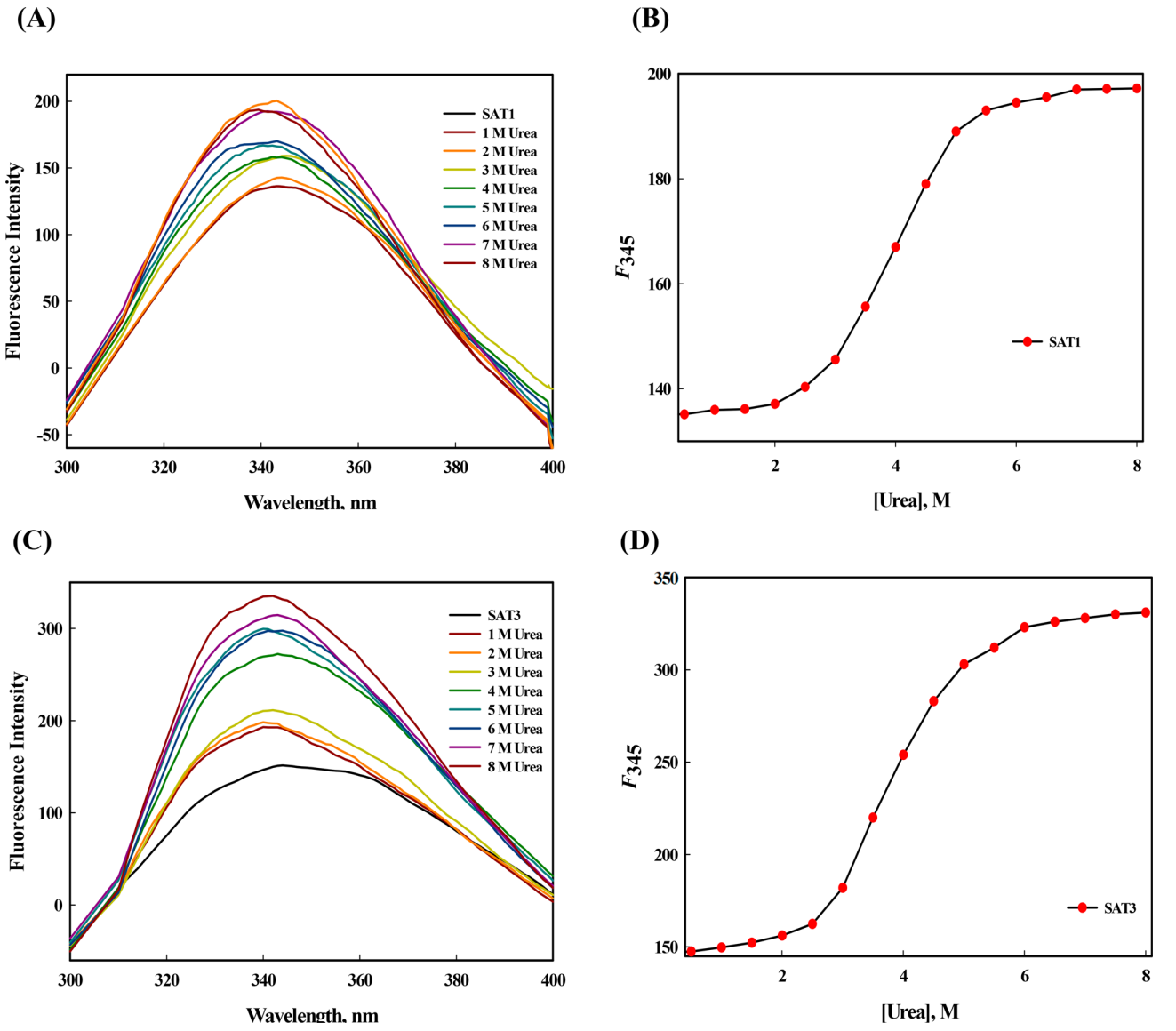

Figure 2. (A) Representative fluorescence spectra of SAT1 recorded as a function of increasing urea concentration at pH 8.0 and 25 °C. (B) Urea-induced transition curve followed by observing changes in F_{345} of SAT1. (C) Representative fluorescence spectra of SAT3 recorded as a function of increasing urea concentration at pH 8.0 and 25 °C. (D) Urea-induced transition curve followed by observing changes in F_{345} in SAT3.

beyond 215 nm. It is seen in Figure 1A and C that, on the addition of urea, SAT1 and SAT3 undergo $\alpha \rightarrow \beta$ transition.

Values of $[\theta]$ at 222 nm were obtained from CD spectra shown in Figure 1A and C and plotted against [urea]. These plots (urea-induced transition curves) for SAT1 and SAT3 are shown in Figure 1B and D, respectively. It is seen in these figures that SAT3 transition starts above 2.0 M urea and is complete around 5.5 M urea (Figure 1D), and, on the other hand, SAT1 undergoes transition from 2.0 M urea, which is complete above 6.5 M urea (Figure 1B). Thus, it seems that SAT1 is more stable than SAT3. As may be seen in Figure 1B and D, there is no change in the secondary structure of SAT1 and SAT3 up to ∼2.5 M urea concentration, but the loss of secondary structure gets started above this concentration, and it continues up to 5.25 M urea. After that, no further change was observed for these proteins. The transition curves of SAT1 and SAT3 show that with an increase in urea concentration, a cooperative transition resulted. We have analyzed the

https://doi.org/10.1021/acsomega.2c02467
ACS Omega 2022, 7, 24626−24637

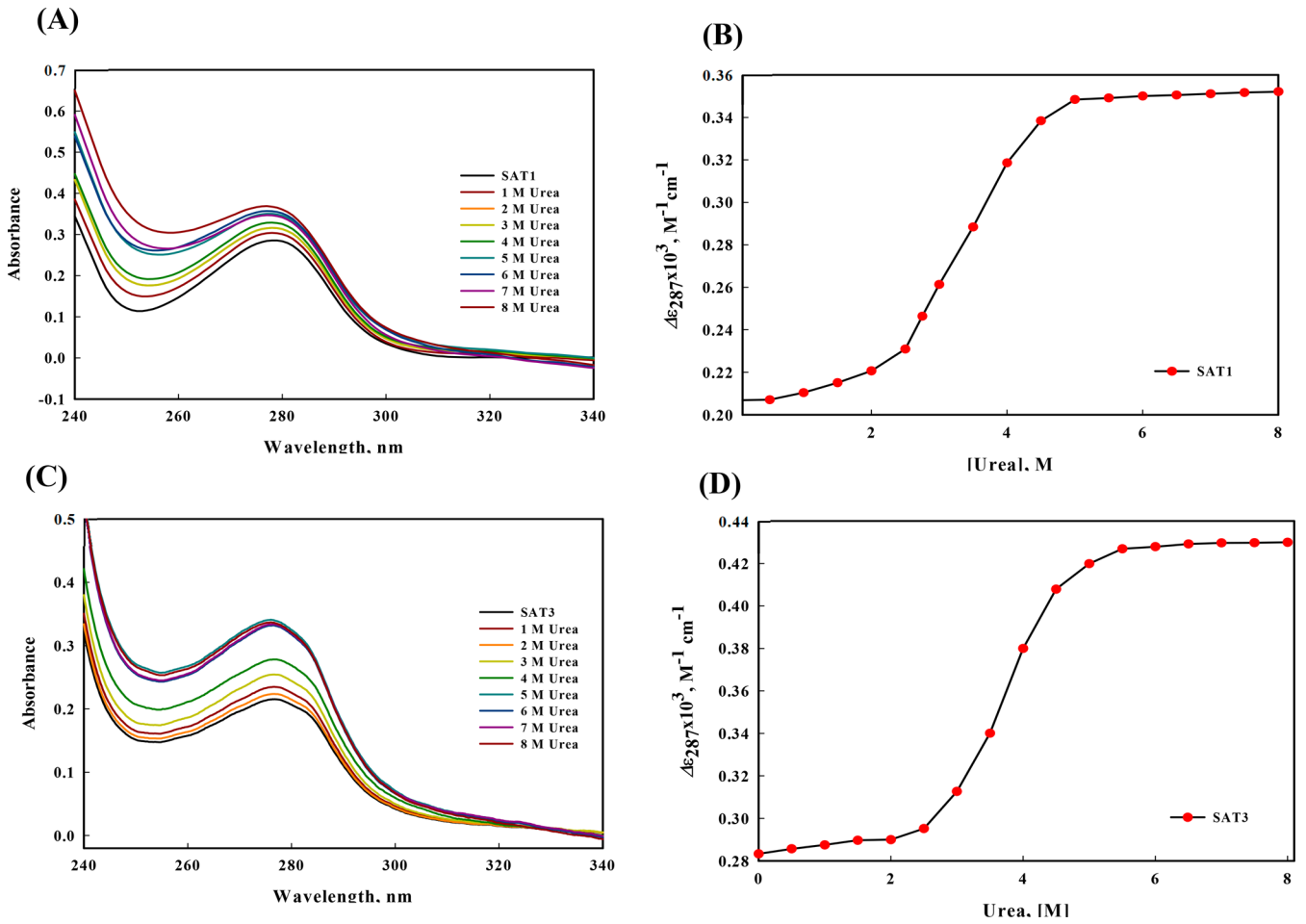

Figure 3. Near-UV absorption spectra of SAT1 and SAT3 at pH 8.0 and 25 °C. (A) Representative absorption spectra of SAT1 recorded as a function of increasing urea concentration. (B) Transition curve of SAT1 obtained by plotting the $\Delta\varepsilon_{287}$ value as a function of [urea]. (C) Representative absorption spectra of SAT3 recorded as a function of increasing urea concentration. (D) Transition curve of SAT3 obtained by plotting the $\Delta\varepsilon_{287}$ value as a function of [urea].

transition curves of both proteins for ΔG_D°, m, and C_m according to eq 2. The thermodynamic parameters are given in Table 1.

3.3. Fluorescence Measurements. Tryptophan fluorescence spectral studies provide information on the tertiary structure of a protein. The fluorescence spectra of SAT1 and SAT3 were measured in the presence of different concentrations of urea at pH 8.0 (50 mM Tris buffer) and 25 °C. The hydrophobic core of globular or multidomain proteins is folded in such a way that tryptophan residues are preferably buried and protected from the solvent. Figure 2A and C show representative fluorescence spectra, and other spectra are shown in Figure S3A and B (Supporting Information). It is seen in these figures that the intensity of the emission peak of SAT1 and SAT3 increased with a blue shift with an increase in the urea concentration. A blue shift of approximately 5 nm was observed. There are two tryptophan residues in SAT1 (Trp195 and Trp255) and three in SAT3 (Trp195, Trp255, and Trp308). Trp195 and Trp255 are buried in both proteins, while Trp308, which is not present in SAT1, is exposed. The observed increase in fluorescence intensity with a blue shift in urea solutions suggests that Trp residue(s) is (are) transferred to a more nonpolar environment.

Figure 2B and D respectively show urea-induced transition curves of SAT1 and SAT3 monitored by F_{345} (Trp-fluorescence emission intensity at 345 nm). The transition curves were analyzed to estimate the values of ΔG_D°, m, and C_m according to eq 2. These thermodynamic parameters are listed in Table 1.

3.4. Absorption Measurements. Near-UV absorbance spectral measurements provide information on the tertiary structure of a protein. Absorption spectra of the SAT1 and SAT3 with different concentrations of urea were measured at pH 8.0 (50 mM Tris buffer) and 25 °C to study the effect of this chemical denaturant on the tertiary structure of both proteins. Figure 3A and C shows representative absorption spectra, and other spectra are shown in Figure S4A and B (Supporting Information). It is seen in these figures that the addition of urea to the protein solution causes an increase in the absorbance near 280 nm. It seems that, as observed from the fluorescence measurements (Figure 2A and C), Trp residue(s) is (are) transferred to a more nonpolar environment on treating proteins with urea.

Figure 3B and D respectively show urea-induced transition curves of SAT1 and SAT3, monitored by $\Delta\varepsilon_{287}$ (difference in molar absorption coefficient in the presence and absence of urea at 287 nm). These transition curves (plots of $\Delta\varepsilon_{287}$ versus [urea]) were analyzed for ΔG_D°, m, and C_m according to eq 2. These thermodynamic parameters are listed in Table 1.

https://doi.org/10.1021/acsomega.2c02467
ACS Omega 2022, 7, 24626−24637

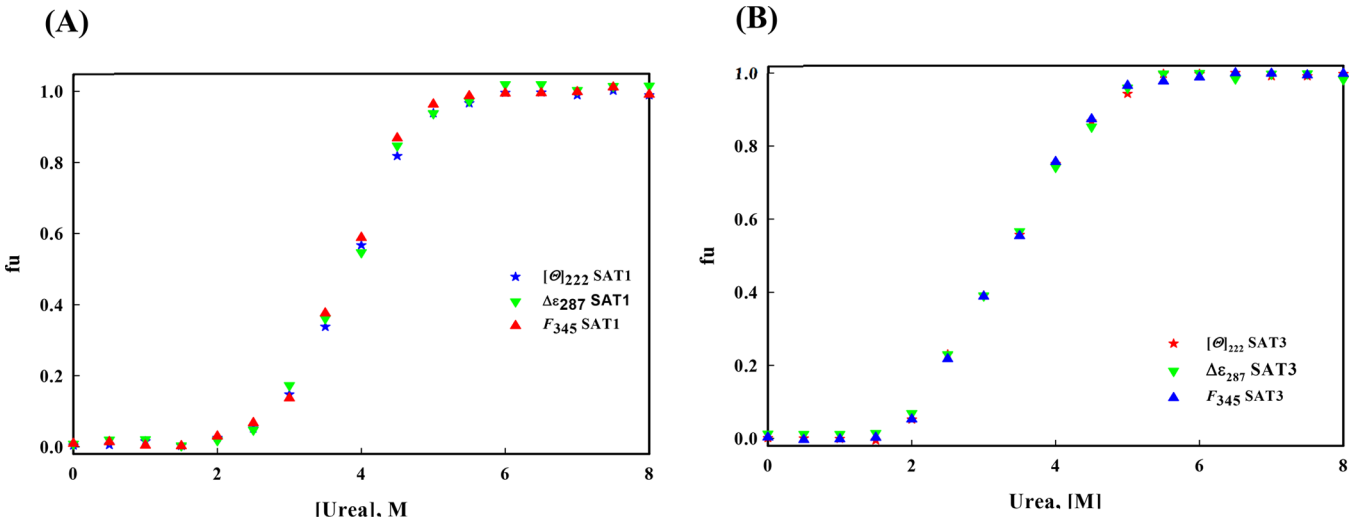

Figure 4. Normalized urea-induced transition curves of SAT1 and SAT3 at pH 8.0 and 25 °C. (A) SAT1 and (B) SAT3. Data were obtained from the analysis of transition curves of $\Delta\varepsilon_{287}$, F_{345}, and $[\theta]_{222}$ to construct plots of f_β of SAT1 and SAT3 versus [urea].

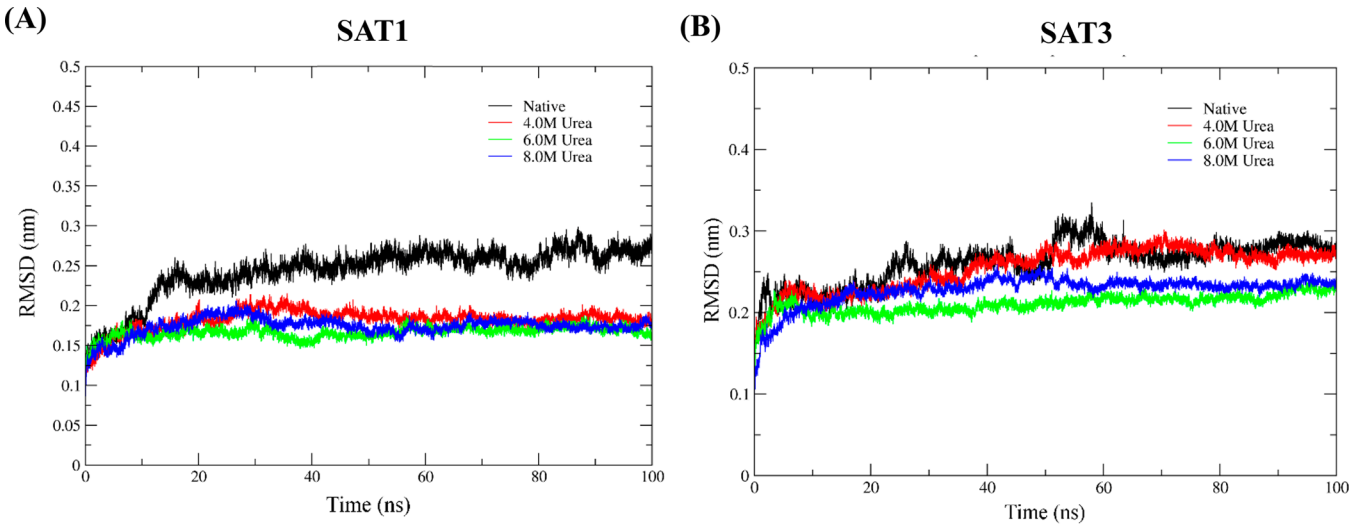

Figure 5. (A) RMSDs of Cα atoms are shown as a function of time for SAT1 in water (black), 4.0 M urea (red), 6.0 M urea (green), and 8.0 M urea (blue) at 300 K. (B) RMSDs of Cα atoms are shown as a function of time for SAT3 in water (black), 4.0 M urea (red), 6.0 M urea (green), and 8.0 M urea (blue) at 300 K.

The isothermal transition of SAT1 and SAT3 induced by chemical denaturant urea were carried out to estimate the protein stability. Normalized transition curves of different physical properties of proteins are used as a test for the two-state transition. The transition curves shown in Figures 1B and D, 2B and D, and 3B and D were normalized to estimate f_β at different urea concentrations using eq 3. These values of f_β are plotted against the concentration of urea in Figure 4 (A and B) that shows a coincidence of normalized transition curves.

In the analysis of urea-induced transition, a few assumptions were made. The first assumption is that the urea-induced transition follows a two-state mechanism. The normalized curves of three optical properties for SAT1 and SAT3 against [urea] (Figures 1, 2, and 3) coincide with each other as shown in Figure 4A and B, respectively suggesting that the first assumption is correct. Furthermore, analysis of transition curves shown in Figures 1−3 according to eq 2 gave identical values of ΔG_D°, m, and C_m for a protein (see Table 1). Almost similar values of each thermodynamic parameter obtained from the analysis of transition curves of three different optical properties support the hypothesis that urea-induced transition of SAT1 and SAT3 follows a two-state mechanism.

The second assumption is that ΔG_D-dependence on [urea] is linear in the entire range. This assumption seems to be valid for many proteins.[30,31] The third assumption is that the optical properties of the protein in the native state (y_N) are independent of [urea], and the denatured state (y_D) is dependent on [urea] in a linear manner.

These stability measurements of SAT1 and SAT3 indicate that SAT1 is more stable than SAT3. CD measurements suggested that urea induces $\alpha \rightarrow \beta$ transition in both proteins. Trp fluorescence and near-UV absorption measurements led us to conclude that this transition is accompanied by the transfer of Trp residue to a more nonpolar environment. To support this conclusion, MD simulation studies were carried out.

3.5. Molecular Dynamics Simulations. As discussed in the Materials and Methods, MD simulations of both SAT1 and SAT3 were performed in the aqueous solution and also in the

https://doi.org/10.1021/acsomega.2c02467
ACS Omega 2022, 7, 24626−24637

presence of urea. MD simulations help to gain atomistic insights of macromolecular systems and their dynamic behavior in various conditions such as mutational effects, ligand interaction, and the effects caused by destabilizers.[32,33] In his review of MD simulations of macromolecules, Martin Karplus, Noble laureate and credited with the first study published on protein folding dynamics in 1977, states the importance of MD simulation methods applied in the study of protein folding/unfolding.[32] In his view, MD simulations have the ability to provide intricate details of "individual particle motions as a function of time", which is a significant observation to study the folding/unfolding of proteins. By studying the trajectories of atomic motions, we can estimate the folding/unfolding pathways and observe the changes occurring in the native structures of the proteins. The structural changes occurring in response to certain events are observed by calculating various geometrical and stereochemical properties of the macromolecules. Such properties include root-mean-square deviation (RMSD) of the atomic positions of the Cα or backbone atoms,[34] radius of gyration (R_g) of the proteins, changes in the atomic position and their effect on residual fluctuations in terms of root-mean-square fluctuation (RMSF), changes in the number of hydrogen bonds during the MD, perturbations in the solvent-accessible surface area (SASA) of the proteins, etc.

3.6. Urea-Induced Conformational Changes in SAT1 and SAT3. To observe the effects of higher concentrations of urea (4.0, 6.0, and 8.0 M) on SAT1 and SAT3, we performed MD simulations of each system for 100 ns in aqueous (0 M urea) and urea solutions. Time evolution plots of RMSD of all the systems (Figure 5A) suggest significant changes in the structure in comparison to the native conformations. Figure 5A shows RMSD values of Cα atoms of SAT1 with the following observations. (i) SAT1 in water shows relatively higher fluctuations in the Cα positions with a high drift up to 15 ns and then achieving balance for the rest of the simulation time. (ii) SAT1 in 4.0 M urea also shows an initial jump of 0.15 nm and then shows a drift of 0.17 nm and then reaches convergence after 40 ns of simulation time. Similarly, (iii) SAT1 in 6.0 M urea also shows an initial peak in the RMSD plot up to 10 ns then reaches convergence. (iv) SAT1 in 8.0 M urea shows similar trends to those in 4.0 and 6.0 M urea. These observations show that urea has a perturbing effect on the conformation of the SAT1 protein. The structure is significantly distorted in the effect of higher concentrations of urea. However, SAT1 in 6.0 and 8.0 M urea shows slightly less perturbance in comparison to SAT1 in a 4.0 M urea solution.

An RMSD plot (Figure 5B) of SAT3 in water and urea at 4.0 and 6.0 M shows similar destabilizing effects on the structure of SAT3 in response to higher concentrations of urea. It was observed that SAT3 in 4.0 M urea solutions shows a high drift of around 0.27 nm up to 50 ns and then reaches convergence trending up to 100 ns. However, SAT3 in 6.0 and 8.0 M urea sees an initial jump of 0.2 nm and then shows a relatively stable pattern of RMSD fluctuation for the rest of the simulation time. The comparison of RMSD plots and average values of RMSD in Table 2 of both SAT1 and SAT3 in 4.0, 6.0, and 8.0 M urea suggests that SAT1 is relatively more stable than SAT3 in solvent conditions.

The radius of gyration (R_g) reflects the changes in the compactness of proteins during folding/unfolding,[35] hence it can be helpful to identify the changes in protein conformation during MD simulations. We calculated the R_g values of both SAT1 and SAT3 in the presence of 4.0 M, 6.0 M, and 8.0 M urea as a function of time. The R_g plot of SAT1 (Figure S5A) in 4.0, 6.0, and 8.0 M urea shows significant changes in the overall compactness of the protein. SAT1 in water (native state) shows a negative drift in the R_g up to 10 ns, then it reaches the convergence and follows the stable conformation up to 100 ns. On the other hand, SAT1 in 4.0 M, 6.0 M, and 8.0 M urea shows the open conformation of the protein, suggesting possible perturbation of the 3D structure of the SAT1. SAT1 in 6.0 M urea shows a higher perturbance in the structure up to 30 ns, then following a stable conformation up to 100 ns. We observed that in comparison to 4.0 and 6.0 M urea, 8.0 M urea has a more stabilizing effect on the structure of the SAT1. The similar trend is observed for SAT3 (Figure S5B) in a 4.0 M urea solution with comparatively lesser deviance than protein in a 6.0 M urea solution. However, for SAT3, 8.0 M urea is causing higher perturbance in comparison to 4.0 and 6.0 M urea, respectively.

Table 2. Average Values of R_g, RMSD, and RMSF for 100 ns of MD Simulations of SAT1 and SAT3 in Aqueous, 4.0 M Urea, 6.0 M Urea, and 8.0 M Urea

				RMSF (nm)		
protein	system	R_g (nm)	RMSD (nm)	chain A	chain B	chain C
SAT1	native	2.587	0.243	0.124	0.136	0.130
	4.0 M urea	2.609	0.182	0.102	0.109	0.107
	6.0 M urea	2.631	0.166	0.114	0.108	0.107
	8.0 M urea	2.595	0.174	0.098	0.108	0.103
SAT3	native	2.581	0.261	0.160	0.135	0.135
	4.0 M urea	2.593	0.254	0.123	0.130	0.114
	6.0 M urea	2.590	0.210	0.107	0.109	0.102
	8.0 M urea	2.599	0.272	0.107	0.116	0.149

Root mean square fluctuation (RMSF) is a helpful parameter to measure the conformational changes at the amino acid level. RMSF plots of both SAT1 and SAT3 show significant changes in the conformation of both the proteins in response to 4.0, 6.0, and 8.0 M urea solutions. Figure 6A shows higher fluctuations in the N-terminal segments of SAT1 followed by a slight stable conformation up to the 200th residue. However, there is a visible fluctuation in the atomic positions of amino acids of SAT1 for all of the monomeric units from the 200th to 225th residue. Similar observations are made for the SAT3 (Figure 6B) in higher concentrations of urea (4.0, 6.0, and 8.0 M). Hydrophobic tryptophan residues Trp195 and Trp295 in SAT1 and SAT3, respectively, show higher fluctuations in the RMSF plot (encircled region in Figure 6A and B), suggesting a relocation of Trp residues toward a more hydrophobic environment.

Figures 7 and 8 show the number of amino acid residues involved in the formation of secondary structure elements for SAT1 and SAT3 in aqueous and urea solutions. For both proteins, a secondary structure plot shows an increase in β sheets in 4.0, 6.0, and 8.0 M urea. Residues involved in β sheet formation are depicted with green color in Figure 8, where an increase in the number of residues involved in β sheet formation is observed.

The superimposed structures of the native SAT1 and SAT3 with the structures extracted from the 100 ns MD trajectories of SAT1 and SAT3 in 4.0, 6.0, and 8.0 M solutions along with secondary structure graphs generated by the STRIDE server

https://doi.org/10.1021/acsomega.2c02467
ACS Omega 2022, 7, 24626−24637

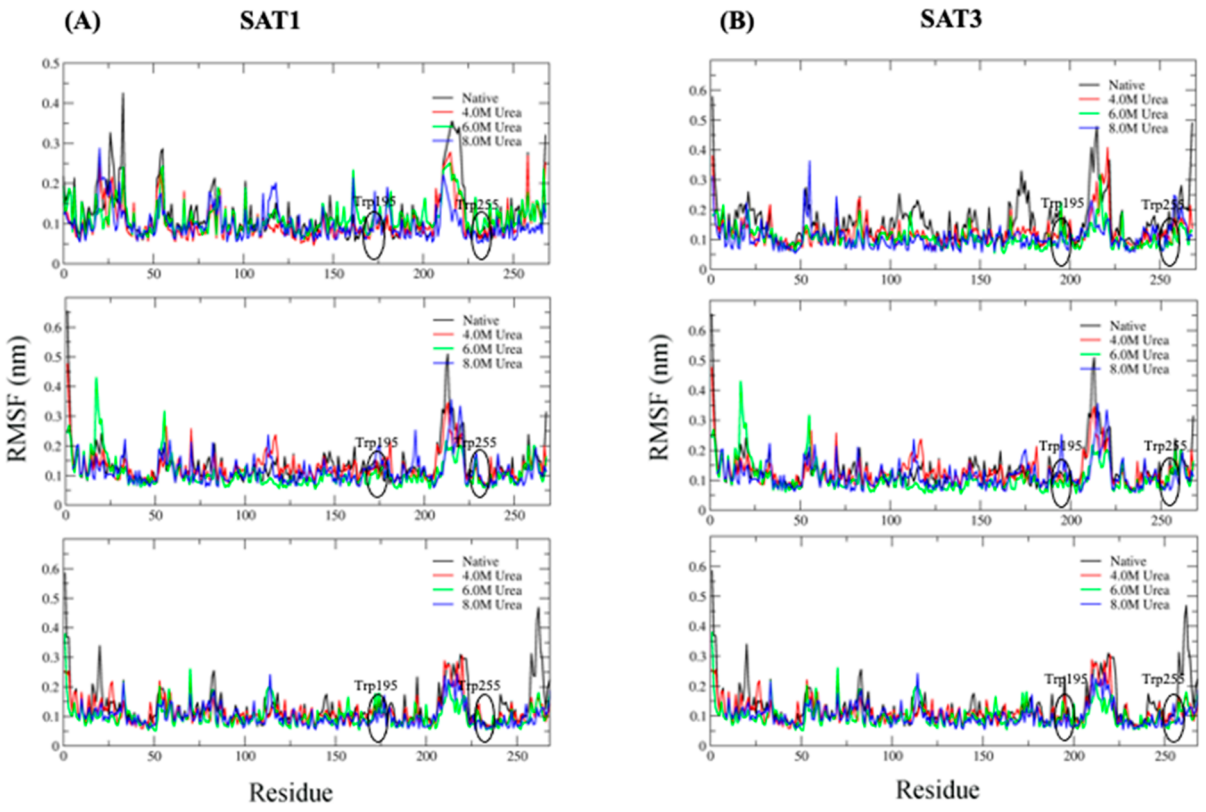

Figure 6. (A) RMSF of amino acid residues of SAT1 in water and different concentrations of urea. SAT1 in water (black), 4.0 M urea (red), 6.0 M urea (green), and 8.0 M urea (blue) at 300 K. Encircled region contains tryptophan 195 and 255 residues. (B) RMSF of amino acid residues of SAT3 in water and different concentrations of urea. SAT3 in water (black), 4.0 M urea (red), 6.0 M urea (green), and 8.0 M urea (blue) at 300 K. Encircled region contains tryptophan 195 and 255 residues.

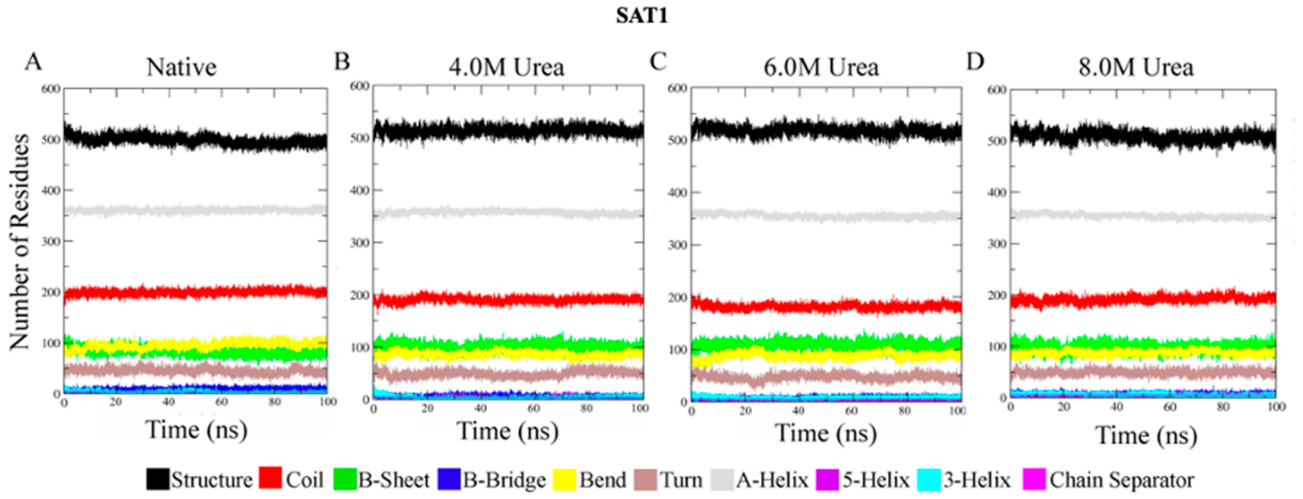

Figure 7. Secondary structure plot of SAT1 in (A) aqueous solution, (B) 4.0 M urea, (C) 6.0 M urea, and (D) 8.0 M urea solutions.

(Figure S6 and S7) suggest an increase in β sheets and a decrease in α helical structure and coil. We also calculated the total solvent accessible surface area for SAT1 (Figure S8A) and SAT3 (Figure S8B), which indicates a significant increase in the SASA in response to 4.0, 6.0, and 8.0 M solution, suggesting an opening of the conformation which occurs in response to the opening of the native conformation. Free energy of solvation (Figure S9A and B) complements the changes in SASA of the SAT1 protein. We observed similar changes in the SASA of SAT3 for 4.0, 6.0, and 8.0 M urea, which is backed by the changes in the free energy of solvation with a significant increase in the values. Changes in the intramolecular hydrogen bonds are also helpful in identifying the structural changes during MD simulations. Hydrogen bond plots (Figures S10 and S11) of both SAT1 and SAT3 for 4.0, 6.0, and 8.0 M urea suggest a decrease in the number of the hydrogen bonds during MD simulation times, indicating possible disruption of the native structure of the protein. The average values of R_g, RMSD, and RMSF for 100 ns MD simulations of SAT1 and SAT3 in the native and urea-induced states are given in Table 2.

https://doi.org/10.1021/acsomega.2c02467
ACS Omega 2022, 7, 24626−24637

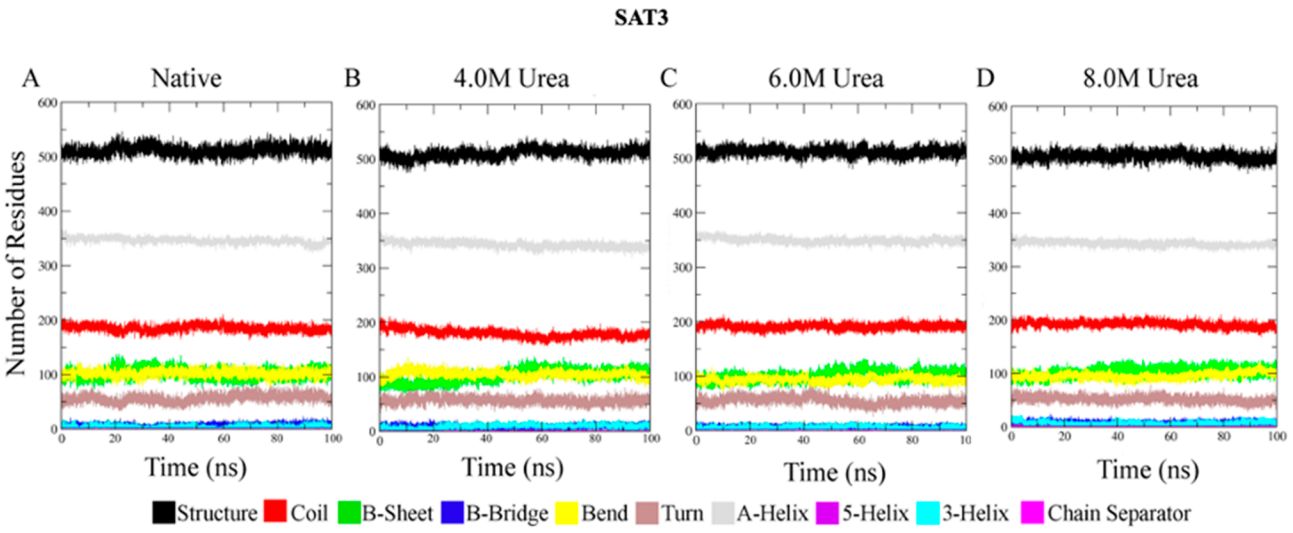

Figure 8. Secondary structure plot of SAT3 in (A) aqueous, (B) 4.0 M urea, (C) 6.0 M urea, and (D) 8.0 M urea solutions.

4. CONCLUSIONS

SAT isoforms are of great biological importance for *E. histolytica* for its growth and survival. However, the structural dynamics of SATs are still not studied well. Here, we have studied the effect of urea on the secondary and tertiary structure of SAT1 and SAT3 to understand its mechanism of folding as well as secondary structural transitions using molecular dynamics. We have observed that the conformational change in SAT1 and SAT3 isoforms in the presence of urea follows a two-state mechanism as revealed by normalized transition curves of all three optical properties $[\theta]_{222}$, F_{345}, and $\Delta\varepsilon_{287}$. Furthermore, this conformational change involves α-helix $\rightarrow$ β-structure transition as revealed by $[\theta]_{222}$ measurements. These *in vitro* observations were complemented by 100 ns MD simulations of both SAT1 and SAT3 in the absence and presence of urea. Thus, these proteins which undergo an α-helix $\rightarrow$ β-sheet transition could be used as models to study neurodegenerative disease pathogenesis. SAT3 is a biologically more important protein, and its function is not regulated through a feedback mechanism of cysteine biosynthesis. *E. histolytica* could not survive if the *SAT3* gene is knockdown, while the organism could survive if *SAT1* and *SAT2* genes are knockdown. Interestingly, SAT3 is less stable then SAT1, although it plays critical role in the survival of *E. histolytica*. Our studies suggested that the structural stability of SAT3 (SAT3 is approximately 2 kcal/mol less stable than SAT1) is compromised by nature, while attaining biologically important functions. The organism has evolved the SAT3 isoform to escape the feedback inhibition by the final product and to keep producing cysteine, but in the process SAT3 compromised its structural stability.

■ ASSOCIATED CONTENT

Supporting Information

The Supporting Information is available free of charge at https://pubs.acs.org/doi/10.1021/acsomega.2c02467.

Figure S1: (A) Gel filtration chromatogram of SAT1: SAT1 is eluted at 72 mL, and purity was checked by SDS-PAGE. (B) Gel filtration chromatogram of SAT3: SAT3 is eluted at 82 mL, and purity was checked by SDS-PAGE. Figure S2: Far-UV CD spectra of SAT1 and SAT3 at pH 8.0 and 25 °C. (A) Far-UV CD spectra of SAT1 were recorded as a function of increasing urea concentration. (B) Far-UV CD spectra of SAT3 were recorded as a function of increasing urea concentration. Figure S3: (A) Fluorescence spectra of SAT1 at pH 8.0 and 25 °C. (B) Fluorescence spectra of SAT3 at pH 8.0 and 25 °C. Figure S4: Absorption spectra of SAT1 and SAT3 at pH 8.0 and 25 °C. (A) Absorption spectra of SAT1 were recorded as a function of increasing urea concentration. (B) Absorption spectra of SAT3 were recorded as a function of increasing urea concentration. Figure S5: (A) Time evolution of radius of gyration (R_g) values during 100 ns of MD simulation for SAT1, in water (black), cosolvent urea 4.0 M (red), 6.0 M (green), and 8.0 M (blue) at 300 K. (B) Time evolution of radius of gyration (R_g) values during 100 000 ps of MD simulation for SAT3, in water (black), cosolvent urea 4.0 M (red), 6.0 M (green), and 8.0 M (blue) at 300 K. Figure S6: (A) Cartoon representation of three-dimensional structure of SAT1 along with secondary structure schema of SAT1 generated by STRIDE web server. (B) SAT1 native structure (magenta) superimposed with SAT1 (cyan) in 4.0 M urea (structure extracted at 100 ns MD simulation time scale) and secondary structure schema. (C) SAT1 native structure (magenta) superimposed with SAT1 (cyan) in 6.0 M urea and secondary structure schema. (D) SAT1 native structure (magenta) superimposed with SAT1 (cyan) in 8.0 M urea and secondary structure schema. Figure S7: (A) Cartoon representation of three-dimensional structure of SAT3 along with secondary structure schema of SAT3 generated by STRIDE web server. (B) SAT3 native structure (magenta) superimposed with SAT1 (cyan) in 4.0 M urea (structure extracted at 100 ns MD simulation time scale) and secondary structure schema. (C) SAT3 native structure (magenta) superimposed with SAT3 (cyan) in 6.0 M urea and secondary structure schema. (D) SAT3 native structure (magenta) superimposed with SAT3 (cyan) in 8.0 M urea and secondary structure schema. Figure S8: (A) Line plot showing changes in solvent accessible surface area (SASA) of SAT1 in aqueous solution, 4.0 M urea, 6.0 M urea, and 8.0 M urea. (B) Line plot showing

https://doi.org/10.1021/acsomega.2c02467
ACS Omega 2022, 7, 24626−24637

changes in SASA of SAT3 in aqueous solution, 4.0 M urea, 6.0 M urea, and 8.0 M urea. Figure S9: (A) Changes in the free energy of solvation of SAT1 in aqueous solution, 4.0 M urea, 6.0 M urea, and 8.0 M urea. (B) Changes in the free energy of solvation of SAT3 in aqueous solution, 4.0 M urea, 6.0 M urea, and 8.0 M urea. Figure S10: Line plot showing number of intramolecular hydrogen bonds for SAT1 in (A) aqueous solution, (B) 4.0 M urea (C) 6.0 M urea, and (D) 8.0 M urea during 100 ns MD simulations. Figure S11: Line plot showing the number of intramolecular hydrogen bonds for SAT3 in (A) aqueous solution, (B) 4.0 M urea, (C) 6.0 M urea, and (D) 8.0 M urea during 100 ns MD simulation (PDF)

AUTHOR INFORMATION

Corresponding Author

Samudrala Gourinath − *School of Life Sciences, Jawaharlal Nehru University, New Delhi 110067, India;* orcid.org/0000-0003-4090-3063; Phone: (+91) 011 2670 4513; Email: sgourinath@mail.jnu.ac.in; Fax: 011 2674 2558

Authors

Danish Idrees − *School of Life Sciences, Jawaharlal Nehru University, New Delhi 110067, India; Faculty of Allied Health Sciences, Shree Guru Gobind Tricentenary University, Gurugram, Harayana 122505, India*

Ahmad Abu Turab Naqvi − *Department of Computer Science, Jamia Millia Islamia, New Delhi 110025, India*

Md Imtaiyaz Hassan − *Centre for Interdisciplinary Research in Basic Science, Jamia Millia Islamia, New Delhi 110025, India;* orcid.org/0000-0002-3663-4940

Faizan Ahmad − *Department of Biochemistry, Jamia Hamdard, New Delhi 110062, India*

Complete contact information is available at: https://pubs.acs.org/10.1021/acsomega.2c02467

Notes

The authors declare no competing financial interest.

ACKNOWLEDGMENTS

D.I. is thankful to University Grant Commission (UGC), India for the award of a D.S. Kothari postdoctoral fellowship (DSK-PDF). F.A. is thankful to the Indian National Science Academy for the award of Senior Scientist Position.

REFERENCES

(1) Nozaki, T.; Asai, T.; Sanchez, L. B.; Kobayashi, S.; Nakazawa, M.; Takeuchi, T. Characterization of the gene encoding serine acetyltransferase, a regulated enzyme of cysteine biosynthesis from the protist parasites Entamoeba histolytica and Entamoeba dispar. Regulation and possible function of the cysteine biosynthetic pathway in Entamoeba. *J. Biol. Chem.* **1999**, *274*, 32445−32452.

(2) Ghosh, S.; Padalia, J.; Moonah, S. Tissue Destruction Caused by Entamoeba histolytica Parasite: Cell Death, Inflammation, Invasion, and the Gut Microbiome. *Curr. Clin Microbiol Rep* **2019**, *6*, 51−57.

(3) Mazumder, M.; Gourinath, S. Structure-Based Design of Inhibitors of the Crucial Cysteine Biosynthetic Pathway Enzyme O-Acetyl Serine Sulfhydrylase. *Curr. Top Med. Chem.* **2015**, *16*, 948−959.

(4) Kumar, S.; Mazumder, M.; Dharavath, S.; Gourinath, S. Single residue mutation in active site of serine acetyltransferase isoform 3 from Entamoeba histolytica assists in partial regaining of feedback inhibition by cysteine. *PLoS One* **2013**, *8*, e55932.

(5) Jeelani, G.; Sato, D.; Soga, T.; Nozaki, T. Genetic, metabolomic and transcriptomic analyses of the de novo L-cysteine biosynthetic pathway in the enteric protozoan parasite Entamoeba histolytica. *Sci. Rep* **2017**, *7*, 15649.

(6) Hussain, S.; Ali, V.; Jeelani, G.; Nozaki, T. Isoform-dependent feedback regulation of serine O-acetyltransferase isoenzymes involved in L-cysteine biosynthesis of Entamoeba histolytica. *Mol. Biochem. Parasitol.* **2009**, *163*, 39−47.

(7) Jeelani, G.; Nozaki, T. Entamoeba thiol-based redox metabolism: A potential target for drug development. *Mol. Biochem. Parasitol.* **2016**, *206*, 39−45.

(8) Kumar, S.; Raj, I.; Nagpal, I.; Subbarao, N.; Gourinath, S. Structural and biochemical studies of serine acetyltransferase reveal why the parasite Entamoeba histolytica cannot form a cysteine synthase complex. *J. Biol. Chem.* **2011**, *286*, 12533−12541.

(9) Doyle, C. M.; Rumfeldt, J. A.; Broom, H. R.; Broom, A.; Stathopulos, P. B.; Vassall, K. A.; Almey, J. J.; Meiering, E. M. Energetics of oligomeric protein folding and association. *Arch. Biochem. Biophys.* **2013**, *531*, 44−64.

(10) Cai, K.; Schirch, D.; Schirch, V. The affinity of pyridoxal 5′-phosphate for folding intermediates of Escherichia coli serine hydroxymethyltransferase. *J. Biol. Chem.* **1995**, *270*, 19294−19299.

(11) Dill, K. A.; Ozkan, S. B.; Shell, M. S.; Weikl, T. R. The protein folding problem. *Annu. Rev. Biophys* **2008**, *37*, 289−316.

(12) Rumfeldt, J. A.; Galvagnion, C.; Vassall, K. A.; Meiering, E. M. Conformational stability and folding mechanisms of dimeric proteins. *Prog. Biophys. Mol. Biol.* **2008**, *98*, 61−84.

(13) Sun, P.D.; Foster, C.E.; Boyington, J.C. Overview of protein structural and functional folds. *Curr. Protoc Protein Sci.* **2004**, *35*, DOI: 10.1002/0471140864.ps1701s35.

(14) Ashraf, G. M.; Greig, N. H.; Khan, T. A.; Hassan, I.; Tabrez, S.; Shakil, S.; Sheikh, I. A.; Zaidi, S. K.; Akram, M.; Jabir, N. R.; Firoz, C. K.; Naeem, A.; Alhazza, I. M.; Damanhouri, G. A.; Kamal, M. A. Protein misfolding and aggregation in Alzheimer's disease and type 2 diabetes mellitus. *CNS Neurol Disord Drug Targets* **2014**, *13*, 1280−1293.

(15) Sweeney, P.; Park, H.; Baumann, M.; Dunlop, J.; Frydman, J.; Kopito, R.; McCampbell, A.; Leblanc, G.; Venkateswaran, A.; Nurmi, A.; Hodgson, R. Protein misfolding in neurodegenerative diseases: implications and strategies. *Transl Neurodegener* **2017**, *6*, 6.

(16) Pan, K. M.; Baldwin, M.; Nguyen, J.; Gasset, M.; Serban, A.; Groth, D.; Mehlhorn, I.; Huang, Z.; Fletterick, R. J.; Cohen, F. E.; et al. Conversion of alpha-helices into beta-sheets features in the formation of the scrapie prion proteins. *Proc. Natl. Acad. Sci. U. S. A.* **1993**, *90*, 10962−10966.

(17) Khan, S.; Vihinen, M. Spectrum of disease-causing mutations in protein secondary structures. *BMC Struct Biol.* **2007**, *7*, 56.

(18) Gross, M. Proteins that convert from alpha helix to beta sheet: implications for folding and disease. *Curr. Protein Pept Sci.* **2000**, *1*, 339−347.

(19) Pace, C. N. Determination and analysis of urea and guanidine hydrochloride denaturation curves. *Methods Enzymol* **1986**, *131*, 266−280.

(20) Idrees, D.; Prakash, A.; Haque, M. A.; Islam, A.; Ahmad, F.; Hassan, M. I. Spectroscopic and MD simulation studies on unfolding processes of mitochondrial carbonic anhydrase VA induced by urea. *J. Biomol Struct Dyn* **2016**, *34*, 1987−1997.

(21) Idrees, D.; Shahbaaz, M.; Bisetty, K.; Islam, A.; Ahmad, F.; Hassan, M. I. Effect of pH on structure, function, and stability of mitochondrial carbonic anhydrase VA. *J. Biomol Struct Dyn* **2017**, *35*, 449−461.

(22) Perez-Iratxeta, C.; Andrade-Navarro, M. A. K2D2: estimation of protein secondary structure from circular dichroism spectra. *BMC Struct Biol.* **2008**, *8*, 25.

(23) Ahmad, F.; Bigelow, C. C. Estimation of the free energy of stabilization of ribonuclease A, lysozyme, alpha-lactalbumin, and myoglobin. *J. Biol. Chem.* **1982**, *257*, 12935−12938.

(24) Santoro, M. M.; Bolen, D. W. Unfolding free energy changes determined by the linear extrapolation method. 1. Unfolding of

phenylmethanesulfonyl alpha-chymotrypsin using different denaturants. *Biochemistry* **1988**, *27*, 8063−8068.
(25) Syed, S. B.; Khan, F. I.; Khan, S. H.; Srivastava, S.; Hasan, G. M.; Lobb, K. A.; Islam, A.; Ahmad, F.; Hassan, M. I. Mechanistic insights into the urea-induced denaturation of kinase domain of human integrin linked kinase. *Int. J. Biol. Macromol.* **2018**, *111*, 208−218.
(26) Sudhaker Dharavath, S. K., Gourinath, S. Crystal structure and novel protecting role of C-terminal tail of E. histolytica Serine Acetyltransferase isoform 3 from feedback inhibition. [UNDER COMMUNICATION].
(27) Greenfield, N. J. Circular dichroism analysis for protein-protein interactions. *Methods Mol. Biol.* **2004**, *261*, 55−78.
(28) Ahmad, F. Protein stability from denaturation transition curves. *Indian J. Biochem Biophys* **1991**, *28*, 168−173.
(29) Kumar, S.; Kumar, N.; Alam, N.; Gourinath, S. Crystal structure of serine acetyl transferase from Brucella abortus and its complex with coenzyme A. *Biochim. Biophys. Acta* **2014**, *1844*, 1741−1748.
(30) Gupta, R.; Yadav, S.; Ahmad, F. Protein stability: urea-induced versus guanidine-induced unfolding of metmyoglobin. *Biochemistry* **1996**, *35*, 11925−11930.
(31) Gupta, R.; Ahmad, F. Protein stability: functional dependence of denaturational Gibbs energy on urea concentration. *Biochemistry* **1999**, *38*, 2471−2479.
(32) Karplus, M.; McCammon, J. A. Molecular dynamics simulations of biomolecules. *Nat. Struct. Biol.* **2002**, *9*, 646−652.
(33) Karplus, M.; Kuriyan, J. Molecular dynamics and protein function. *Proc. Natl. Acad. Sci. U.S.A.* **2005**, *102*, 6679−6685.
(34) Sargsyan, K.; Grauffel, C.d.; Lim, C. How molecular size impacts RMSD applications in molecular dynamics simulations. *J. Chem. Theory Comput.* **2017**, *13*, 1518−1524.
(35) Lobanov, M. Y.; Bogatyreva, N. S.; Galzitskaya, O. V. Radius of gyration as an indicator of protein structure compactness. *Mol. Biol.* **2008**, *42*, 623−628.

https://doi.org/10.1021/acsomega.2c02467
ACS Omega 2022, 7, 24626−24637